agriculture

Article

Research on the End Effector and Optimal Motion Control Strategy for a Plug Seedling Transplanting Parallel Robot

Xiong Zhao [1,2], Di Cheng [1], Wenxun Dong [1], Xingxiao Ma [1], Yongsen Xiong [3] and Junhua Tong [1,2,*]

1 Faculty of Mechanical Engineering and Automation, Zhejiang Sci-Tech University, Hangzhou 310018, China
2 Zhejiang Province Key Laboratory of Transplanting Equipment and Technology, Hangzhou 311121, China
3 Key Laboratory of Crop Harvesting Equipment Technology of Zhejiang Province, Jinhua 321017, China
* Correspondence: jhtong@zstu.edu.cn; Tel.: +86-8684-3756

Abstract: Due to the phenomenon of holes and inferior seedlings in trays, it is necessary to remove and replenish unqualified seedlings. The traditional operation is labor-intensive, and the degree of mechanization is low. This paper took broccoli seedlings as the research object and developed an image recognition system suitable for seedling health recognition and pose judgement, researched and designed a plug-in end effector that reduces leaf damage, and conducted orthogonal tests to obtain a substrate parameter combination containing the moisture content, seedling age, and transplanting acceleration suitable for culling operations. A parallel robot kinematics and dynamics model was built. The fifth degree B-spline curve was used to construct the joint space motion curve for seven nodes, and the motor speed, torque, and end-effector acceleration were used to construct the joint space motion curves. The end-effector acceleration was the constraint condition to plan the optimal trajectory of the joint space in time, and the optimal time was obtained using the artificial fish swarm–particle swarm hybrid optimization algorithm. A single operation time was greatly reduced; the whole machine was systematically built; the average time of single-time seedling removal was measured; and the transplanting efficiency of the whole machine was high. In the seedling damage rate gap test, the leaf damage rate was low. This research provides a reference for the localized development of greenhouse high-speed and low-loss seedling removal equipment.

Keywords: growth pose judgement; removal and supplementation of seedlings; end effector; delta robot; artificial fish swarm–particle swarm optimization algorithm; optimal time trajectory planning

Citation: Zhao, X.; Cheng, D.; Dong, W.; Ma, X.; Xiong, Y.; Tong, J. Research on the End Effector and Optimal Motion Control Strategy for a Plug Seedling Transplanting Parallel Robot. *Agriculture* **2022**, *12*, 1661. https://doi.org/10.3390/agriculture12101661

Academic Editors: José Lima, José Boaventura Ribeiro da Cunha, Antonio Valente and Filipe Neves dos Santos

Received: 9 September 2022
Accepted: 28 September 2022
Published: 10 October 2022

1. Introduction

China is the largest producer and consumer of vegetables in the world. Vegetable output increased from 553 million tons in 2009 to nearly 692 million tons in 2017, with an output of 1640 kg per unit and an average per capita occupancy of 570 kg [1]. As a key link in the vegetable production process, vegetable seedlings are not only the basis for ensuring the healthy development of the vegetable industry but can also better maximize the benefits of vegetable production [2–4]. In plug seedling technology, only one seed is placed in one hole, which can realize seedling formation at once [5,6]. The plug seedling method can effectively reduce the number of seeds sown, and the characteristics of individual plants are also conducive to the production environment of plants. At the same time, this method makes the germination quality of seeds high, making them suitable for long-distance transportation and intensive production and management [7,8]. However, due to the germination rate of seeds and the environment of seedlings, holes often appear in the trays [9]. These holes seriously affect the subsequent sale and transplanting of plug seedlings. The problems of strong manual dependence, high labor intensity, low degree of mechanization, and insignificant comprehensive economic benefit exist in plug seedling picking and transplantation in China [10]. With the development of agricultural mechanization in China, automatic seedling removal and supplementation technology has wide application prospects [11,12].

There have been many studies on greenhouse plug seedling removal and supplementation equipment. Agricultural-technology-developed countries have advanced equipment for removing and supplementing seedlings. A pinacate-type pick-up device for automatic transplanting of seedlings in greenhouse was designed by H Mao. [13], which detects the status of each seedling via a built-in imaging system, extracts the plant from the donor tray with multiple grippers, assisted by a method that ensures that the tray is in a 100% filling state after transplanting and seedling selection, and the overall efficiency can reach 30,000 plants/h. Additionally, a push rod system below removes inferior seedlings to fill the healthy ones. Another Netherlands company, Visser, designed and developed pot tray seedling grading equipment [14]. The end effector lifts the plug seedlings, and visual inspection is carried out on the side; different types of seedlings are classified, the unqualified seedlings are weeded out, and the qualified seedlings are then placed into the target tray. Six end effectors were equipped at the same time, which greatly improved operation efficiency.

In order to solve the major problems posed by utilizing cable-driven robots for agricultural or gardening purposes, Vafapour, R. represented an agriculture four-cable robot for some agricultural activities [15]. He revealed the workspace limitations for the robot's end effector to be restricted. Focused on the adjustability of its several joints, a model is presented to achieve an ideal design for the robot's motor-to-pulley mechanism.

An improved greedy simulated annealing algorithm (IGSA) based on the MTSP mode was proposed by Junhua, T. for path optimization [16]. One manipulator had five end effectors attached to it. When the machine starts the re-plug operation, the manipulator moves to the source tray to grasp the entire row of healthy seedlings. The operation of grasping the seedlings is not allowed when an end effector identifies a vacant cell. Then, the manipulator moves to the target tray with the healthy seedlings. The end effectors in the manipulator release the healthy seedlings into the several vacant cells of the target trays. In the end, the manipulator returns to the source tray with empty end effectors. Subsequently, the seedlings are grasped in rows from top to bottom. This automated transplanting of seedlings matched end effectors and visual recognition systems. The removal and supplementation of seedling technology is relatively mature and reliable, but the price is high, and it is generally set up with multiple transplanting claws to identify the state of the seedlings and operate separately, which improves efficiency but leads to the bulkiness of the machine.

Ding Yuhua [17] designed a fully automatic transplanting machine integrating image recognition and processing, plug transportation, and plug seedling removal and supplementation. The photoelectric sensors that the machine is equipped with can identify the existence of plug seedlings and communicate with the lower part of the machine. The lower transplanting system can receive the processing results for removal and supplementation, and the whole machine can cycle transplanting production in combination with sensors and other electronic control components. The overall gantry structure of the equipment is relatively large, and the end-effector design is not light enough. Jiang et al. [18,19] designed and developed a kind of greenhouse pot seedling automatic transplanting equipment prototype, which was controlled by a PLC system and combined with a seedling visual recognition system, and the recognition accuracy rate reached 90%, but the recall rate only reached 64%. Four different crops were tested and transplanted, and the success rate of transplantation was able to reach more than 90%. At the same time, two clamping end effectors were designed, which have the advantages of adjustable insertion depth and angle, so that the clamped seedling remains intact during the transplanting process. However, the use of pin-clamp end effectors will inevitably cause damage to the leaves, and the recognition recall rates are very low. Xin, J. [20] designed a five-bar and fixed-axis gear train picking mechanism suitable for the operation of plug seedlings using machine vision technology to realize the segmentation of plug seedlings and obtained the actual position of plant rhizomes through program processing to ensure the operation of the end effector.

This mechanism can accurately move to the top of the seedlings for transplanting, but the designed parallel transplanter had a small working space and certain limitations.

The automated transplanting of seedlings was lightweight, and sensors were used to identify whether there is a seeding in a plug, but it is impossible to distinguish the posture of seedlings in the acupuncture plate. The accuracy of the visual recognition system is relatively low, and there has been less research on identifying the posture of seedlings, while the corresponding end effector is limited by the lack of motion space of the mechanism form and can damage seedlings easily.

Fan et al. [21] researched and developed a vacuum suction seedling transplanter, which sucked the whole seedling for transplanting through vacuum suction. The experiment verified that the transplanting success rate and transplanting efficiency were significantly improved. However, this equipment was only suitable for rice seedlings, and transplanting flower and vegetable seedlings caused damage easily. Vacuum suction seedling transplanters have good prospects, but due to the different suction forces required for different seedlings, vacuum suction should be adjusted accordingly, and one machine can only achieve the transplanting of specific seedlings.

Hu Shuangyan [22] designed a flexible clamping device using a Cam-guide rod for pepper plug seedlings. These types of linkage end effectors have a small working space and certain limitations. Isaac Ndawula [23] designed a double planar scissor mechanism which is installed on two identical 2DOF translational parallel robots to fetch and transplant seedlings. This end effector has six grippers and can transplant six seedlings at once both when two parallel robots are close and when they are far away. This mechanism cannot achieve the grasping of individual seedlings separately, which is incompatible with the removal and supplementation of seedlings. Tian Subo [24] designed a transplanter for transplanting plug seedlings into pots. The main body of the equipment adopted a three-degrees-of-freedom gantry, and three end effectors were installed on it to quickly open and close to achieve efficient transplanting. However, all of these have low actual operating efficiency, or the size of the mechanism is huge and cannot be adjusted according to the growth state of the seedlings.

In the existing research, greenhouse removal and replenishment equipment have problems such as low operation efficiency and huge structures, and the end effector can easily damage seedlings [25]. Aiming to address the deficiencies of the existing research, this article outlines how we mainly set up a closed image acquisition system, conducted a three-level and three-factor orthogonal test to obtain the optimal combination of parameters, used the PSO–AFSA algorithm and fifth degree B-spline curve to search for the optimal time in one single operation, built the whole machine, and carried out the related experiments. This research provides a reference for the localized development of greenhouse high-speed and low-loss seedling removal equipment.

2. Materials and Methods

2.1. Recognition and Pose Judgement of Plug Seedlings

Due to factors such as seeding technology and plant growth status, seedling leaves often cross borders on one side. Seedling leaves are easily damaged if the end effector is designed without considering the possibility of seedling leaves getting stuck during the process of crossing borders. Therefore, it is necessary to recognize and judge the growth position and orientation of seedling leaves.

The test objects were broccoli plug seedlings; the standard tray is 566 mm long and 286 mm wide, the size of the top of the tray is 30 mm × 30 mm, the size of the lower part of the tray is 20 mm × 20 mm, the tray height is 42 mm, and there are a total of 128 holes. They were sown by Hangzhou Xiaomiao Agricultural Technology (Hangzhou, China) on 1 November 2021 and retrieved after 10 days. At this time, the broccoli seedlings were in a growing period, the seedlings had 2–3 leaves, and the leaf area was small, which basically means that they will not produce the phenomenon of adjacent leaves blocking each other, so the identification difficulty is low.

To facilitate the extraction of seedling growth information in the tray, this paper adopts the method of dual-threshold segmentation. The dual threshold is set as T1 and T2. When the image pixels are smaller than T1 or larger than T2, the pixels are set to 0, while in the interval range, they are set to 255. After greying, threshold segmentation is performed, as shown in Figure 1a. The obtained binary image can basically distinguish the basic contour of the tray. Some of the binary pixel points of the substrate are stored in the cavity. First, the corrosion operation is adopted to eliminate the large area, and then, the small area is opened and calculated to basically obtain the binary image of the frame of the tray, as shown in Figure 1b.

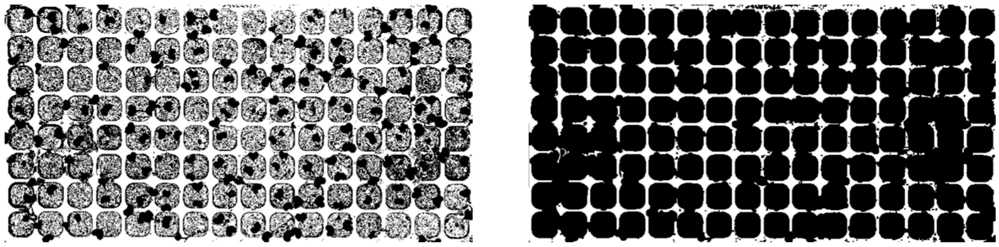

(a) (b)

Figure 1. Threshold segmentation and borderline binarization: (**a**) tray threshold segmentation and (**b**) tray binarization.

Each hole of the standard tray has the same length and width, and the holes are arranged regularly in the tray. The pixel values projected in the horizontal and vertical directions have regular peaks and troughs so that the position of the edge line of the tray can be obtained. The seedling leaves are extracted using the HSV color space, the extracted leaf features are transformed into binarized images, the small area connected domains are removed, and the binarized images of seedling leaves are merged with the tray borders, as shown in Figure 2.

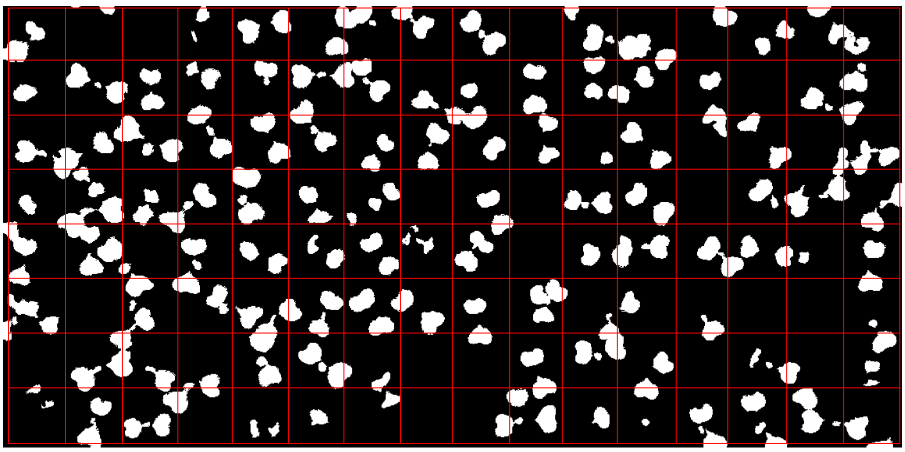

Figure 2. Seedling binary and tray frame image.

According to the leaf area and the position relationship between the leaf and the inner frame of the tray, the seedlings are divided into four types. If the leaf area exceeds 100 mm^2, the seedlings are considered healthy, and if the leaf area is less than 100 mm^2, the seedlings are considered inferior, as shown in Figure 3a. Next, the distance between the centroid of the leaf and the hole center of the tray is determined. If it is less than 10 mm and the secant between the binary image and the tray boundary exceeds 12 mm, it is considered to be out of bounds. The cross-border is divided into two forms: “left and right cross-border” and “up and down cross-border”, as shown in Figure 3b,c. Horizontal grabbing is used for the left–right cross-border, and vertical grabbing is used for the up and down cross-border.

If the pixel value between the image and the secant line of the tray boundary is less than 12 mm, it can be captured in any direction, as shown in Figure 3d. If the pixel value between the image and the secant line of the tray boundary is larger than the threshold range, it indicates that the seedlings are growing very close to the corners, and to ensure the integrity of the transplanted seedlings, they are also considered inferior seedlings.

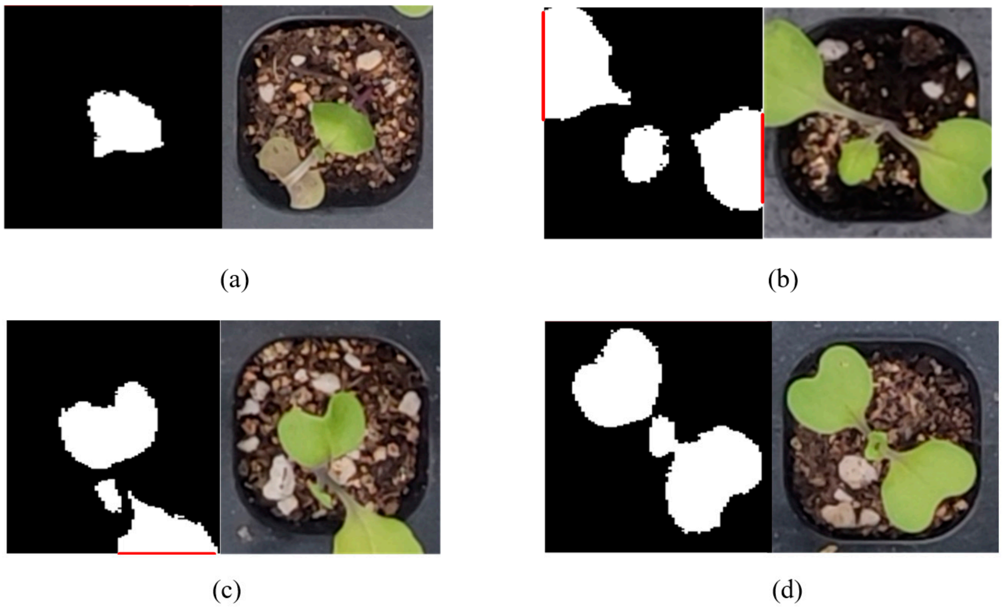

Figure 3. Four kinds of seedling identification results: (**a**) inferior seedlings, (**b**) left and right cross-border healthy seedlings, (**c**) up and down cross-border healthy seedlings, and (**d**) healthy seedlings that do not cross the border.

2.2. Design of the End Effector and Analysis of Factors for Removing and Supplementing Seedlings

The clamping-type end effector is obliquely inserted into the seedling at a fixed angle; the seedling is removed by utilizing the friction force generated by the extrusion of the seedling-taking claw and the substrate, and the damage to the substrate in the clamping process is small, so the clamping-type end effector is suitable for removal and supplementation [21]. After multiple adjustments, a single-degree-of-freedom cylinder-driven plug-in end effector was designed, which is composed of a double-acting cylinder, a connecting plate, a side plate, a miniature linear slide, a seedling picking claw, and a seedling blocking plate. The engineering design is shown in Figure 4a, and the real view is shown in Figure 4b.

To grasp the seedlings in different growth positions and make the end effector grasp horizontally and vertically, a rotating cylinder that can rotate back above the end effector is installed, and a magnetic switch to make the cylinder rotate back and forth 90 degrees is installed.

The specific working principle of the end effector is shown in Figure 5.

(1) The work cycle of removing and supplementing seedlings starts. The end effector runs above the target position, and the cylinder is in the contracting state. The seedling claw follows the sliding rail to the inside of the seedling stopper, as shown in Figure 5a.
(2) The cylinder outstretches, claws out, and is inserted into the seedling substrate from both sides of the bowl, as shown in Figure 5b.
(3) The end effector of the robot is raised to remove the seedling from the supplying tray, as shown in Figure 5c.
(4) The end effector of the robot descends to the target position, the cylinder contracts, the seedling falls into the planting tray due to gravity, and one transplanting seedling process is completed, as shown in Figure 5d,e.

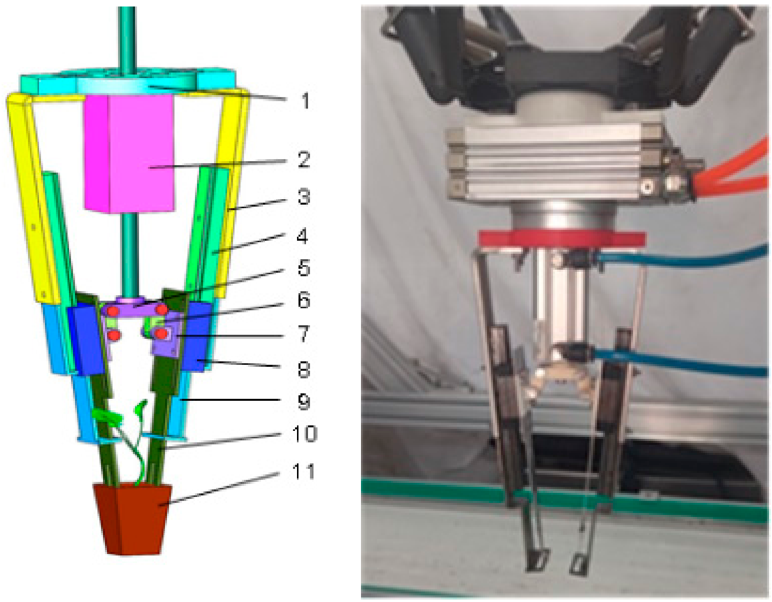

(**a**) (**b**)

Figure 4. (**a**) A 3D modeling view of the end effector. (**b**) Finished product view of the end effector. 1. Cylinder connecting plate; 2. double-action cylinder; 3. side plate; 4. slide rail; 5. cylinder tail; 6. connecting rod; 7. slider plate; 8. slider; 9. seedling stopper; 10. seedling claw; 11. plug seedling.

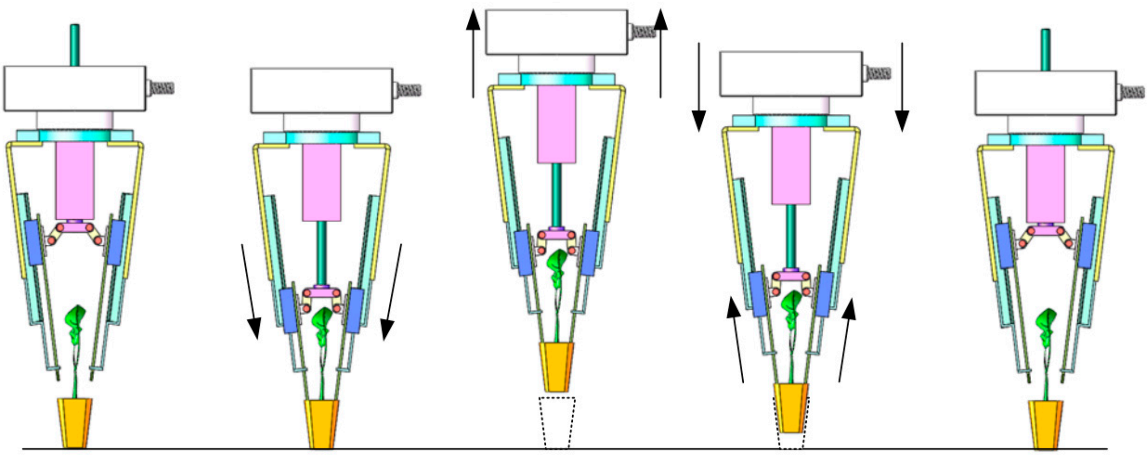

(a) (b) (c) (d) (e)

Figure 5. The transplanting process of the end effector. (**a**) Initial state; (**b**) the seedling is clawed out; (**c**) the end effector is raised; (**d**) the end effector and claw are contracted; (**e**) replenishment is completed.

As is shown in Table 1. This paper proposes a multiobjective orthogonal experiment with three factors and three levels of substrate moisture content, seedling age, and end-effector acceleration. The effects of various factors on the transplanting performance are comprehensively considered. The transplanting success rate of healthy seedlings, retention rate of substrates, transplanting success rate of inferior seedlings, and substrate cleanness rate are selected as the four indicators to test the transplanting performance during the transplanting process [24].

Table 1. Parameters of the orthogonal experiment.

No.	A Substrate Moisture Content (%)	B Seedling (Age/d)	C Transplanting Acceleration (mm/s^2)
1	60–70	20	20
2	70–80	25	30
3	80–90	30	40

The transplanting success rate of healthy seedlings is defined as the percentage of the number of seedlings that do not drop out with respect to the total number of healthy seedlings transplanted. The substrate retention rate is the percentage of the total mass of seedlings after transplanting with respect to the total mass of seedlings before transplanting. The transplanting success rate of inferior seedlings refers to the percentage of the number of seedlings that do not drop out with respect to the total number of inferior seedlings transplanted. The substrate cleanness rate is the percentage of the mass of the inferior seedlings after picking with respect to the original mass of the inferior seedlings.

In the experiment, the degree of membership is used to evaluate the index. The degree of membership of the index with the best maximum value is (index value–index minimum value)/(index maximum value–index minimum value). The most important indicator of removing and supplementing seedlings is the transplanting success rate of healthy seedlings and inferior seedlings, followed by the substrate retention rate and substrate cleanness rate, so the weighted factor of the transplanting success rate of healthy seedlings and inferior seedlings is set to 0.3, and the weighted factor of the substrate retention rate and substrate cleanness rate is set to 0.2, with a full score of 1. The comprehensive score is expressed as Equation (1).

$$\sum_i = 0.3 \times \tau_a + 0.3 \times \tau_b + 0.2 \times \tau_c + 0.2 \times \tau_d \quad (1)$$

where τ_a is the membership degree of the transplanting success rate of healthy seedlings, τ_b is the membership degree of the transplanting success rate of inferior seedlings, τ_c is the membership degree of the substrate retention rate, and τ_d is the membership degree of the substrate cleanness rate.

SPSS 18.0 software (San Jose, CA, USA) was used to analyze the extreme deviation and variance of the test results [26]. Table 2 shows the orthogonal test results of three factors and three levels of transplanting performance. Among them, k1, k2, and k3 represent the average comprehensive scores of moisture, temperature, and humidity in the first, second, and third levels, respectively. For example, the value of k1 is equal to the average value of comprehensive score when the number is 1 in the column with experiment number A. R represents the range. For example, the valve of R is equal to the maximum of k1, k2, k3 minus the minimum of k1, k2, k3. Table 3 shows the variance analysis of each index. The column labeled Prominent, the more asterisks, the greater the effect of each factor on the transplanting performance of the end effector. The results of the orthogonal test and variance analysis show that the order of the effect of each factor on the transplanting performance of the end effector is A (moisture content of substrate) > C (transplanting acceleration) > B (seedling age). The L9(3^4) orthogonal test results show that the parameter combination A1B2C2 with a comprehensive score of 0.87 is the optimal combination, that is, the substrate moisture content is 60–70%, the seedling age is 25 days, and the transplanting acceleration does not exceed 30 mm/s^2. Under this condition, the transplanting success rate of the two types of seedlings and the retention rate and the integrity rate of the substrate are high, and they are suitable for the operation of removing and supplementing seedlings.

Table 2. Extreme deviation analysis.

NO.	A	B	C	Transplanting Success Rate of Healthy Seedlings (%)	Transplanting Success Rate of Inferior Seedlings (%)	Substrate Retention Rate (%)	Substrate Cleanness Rate (%)	Comprehensive Score
1	1	1	1	87.50	85.93	87.54	87.37	0.695
2	1	2	2	96.88	92.19	85.32	83.14	0.871
3	1	3	3	89.06	85.94	82.36	82.26	0.447
4	2	1	2	89.06	87.50	85.83	82.66	0.624
5	2	2	3	85.94	84.38	83.28	81.45	0.419
6	2	3	1	85.94	82.81	86.77	82.48	0.501
7	3	1	3	81.25	78.13	82.26	79.58	0.123
8	3	2	1	84.38	82.81	83.41	80.15	0.323
9	3	3	2	85.94	84.38	80.74	74.42	0.219
k1	0.671	0.481	0.506					
k2	0.515	0.538	0.571					
k3	0.222	0.389	0.330					
R	0.449	0.149	0.241					

Table 3. Analysis of variance.

Source	Squares	Degrees of Freedom	Mean Square	Value of F	Value of p	Obvious
Model	0.441	6	0.074	38.466	0.026	*
A	0.314	2	0.157	82.112	0.009	**
B	0.033	2	0.017	8.660	0.104	
C	0.094	2	0.047	24.625	0.039	*
Error	0.004	2	0.002			
Determining coefficient	R^2 = 0.957					

2.3. Modeling of the Delta Robot for Removing and Supplementing Seedlings

A sketch of the delta robot structure is shown in Figure 6. The static platform and dynamic platform external circle radii R and r are set, respectively, where A_iB_i is the active arm, the rod length is l_1, the follower lever parallelogram mechanism is simplified to a rod, B_iC_i is the follower lever, and the length is l_2. The angle between the X-axis and OA_i and the angle between the X-axis and $O'C_i$ is φ_i, and the angle formed by AB and the XY plane is q_i.

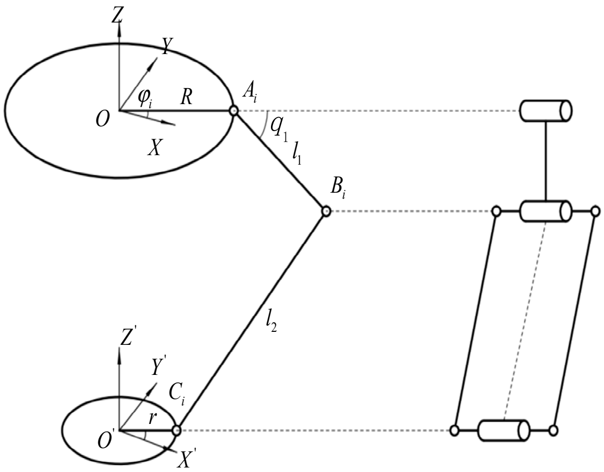

Figure 6. Model of the parallel mechanism.

The position vector of the center of the moving platform is given in the coordinate system. By studying the seal vector loop of a single branch, the geometric relationship can be expressed as Equation (2).

$$OO' = OA_i + A_iB_i + B_iC_i + C_iO \tag{2}$$

Each coordinate point is deduced to obtain Equation (3).

$$[(R+l_1\cos q-r)\cos\varphi_i-X]^2+[(R+l_1\cos q-r)\sin\varphi_i-Y]^2+(l_1\sin q+Z)^2=l_2^2 \quad (3)$$

To facilitate the calculation, the above formula can be simplified as $a\sin q+b\cos q=c$, where

$$\begin{array}{l} a=2l_1Z \\ b=2(R-r)l_1-2Xl_1\cos\varphi_i-2Yl_1\sin\varphi_i \\ c=l_2^2+2(R-r)(X\cos\varphi_i+Y\sin\varphi_i)-(R-r)^2 \\ -l_1^2-X^2-Y^2-Z^2 \end{array}$$

The inverse kinematics solution is expressed as Equation (4).

$$q_i=2\arctan\frac{a\pm\sqrt{a^2+b^2-c^2}}{b+c}, i=1,2,3 \quad (4)$$

The Jacobian matrix is one of the most important parameters in robot motion analysis and control [27] and represents the mapping relationship between the joint velocity and end velocity of the mechanism, i.e., $s_i=O'C_i-(O'O+OA_i+A_iB_i)$.

According to the vector relationship of the single-chain closed loop, Equation (5) is obtained:

$$s_i=\begin{bmatrix}\dot{X}\\ \dot{Y}\\ \dot{Z}\end{bmatrix}+\begin{bmatrix}l_1\sin q_i\cos\varphi_i\\ l_1\sin q_i\sin\varphi_i\\ l_i\cos q_i\end{bmatrix}\dot{q}_i=\dot{X}_n+b_i\dot{q}_i \quad (5)$$

where $\dot{q}=\begin{bmatrix}\dot{q}_1 & \dot{q}_2 & \dot{q}_3\end{bmatrix}^T$ is the angular velocity of each active arm. The Jacobian matrix is obtained as Equation (6).

$$J=-\begin{bmatrix}s_1^T\\ s_2^T\\ s_3^T\end{bmatrix}^{-1}\begin{bmatrix}s_1^Tb_1 & 0 & 0\\ 0 & s_2^Tb_2 & 0\\ 0 & 0 & s_3^Tb_3\end{bmatrix} \quad (6)$$

The dynamic output torque of the delta robot mainly includes the inertial term and gravity term, and the input torque is the driving torque of the motor. The complete rigid body dynamic model of the system is [28]:

$$\sum_{i=1}^{3}\tau_{a,i}+\sum_{i=1}^{3}\tau_{b,i}+\tau_{move}=0 \quad (7)$$

where $\tau_{a,i}$ is the torque of the active arm, $\tau_{b,i}$ is the torque of the follower arm, and τ_{move} is the torque of the moving platform.

The application of the virtual work principle to bodies can be expressed as Equation (8).

$$\sum_{i=1}^{3}[(m_i\ddot{x}_i-F_i)\delta x_i+(I_i\dot{\omega}_i+\omega_i\times I_i\omega_i-T_i)\delta\phi_i]=0 \quad (8)$$

where m_i and I_i are the mass and rotation of i, respectively, and $\ddot{x}_i$, $\dot{\omega}_i$ and ω_i are the center of mass acceleration, angular acceleration, and angular velocity of i, respectively. F_i and T are the external force and torque of i, respectively. δx_i and $\delta\phi_i$ are the virtual displacements of i.

The driving torque of the active joint obtained through deduction is:

$$\tau=(I_{at}+J^Tm_{movet}J)\ddot{q}+J^Tm_{movet}\dot{J}\dot{q}-J^Tm_{moveg}\begin{bmatrix}0\\ 0\\ -g\end{bmatrix}-G_{ag}$$

where m_a is mass of the active arm, m_b is mass of the spherical hinge, m_c is mass of the follower arm, I_m is rotational inertia of the motor, and m_{move} is the total mass of the moving platform and load:

$$\begin{aligned}
&m_{movet} = m_{move} + m_c \\
&I_{at} = \begin{bmatrix} I_{at1} & 0 & 0 \\ 0 & I_{at2} & 0 \\ 0 & 0 & I_{at3} \end{bmatrix} \\
&I_{ati} = I_m + l_1^2\left(\frac{m_a}{3} + m_b + \frac{2}{3}m_c\right) \\
&G_{ag} = l_1\left(\frac{1}{2}m_a + m_b + \frac{1}{2}m_c\right)g\begin{bmatrix} \cos q_1 & \cos q_2 & \cos q_3 \end{bmatrix}^T \\
&m_{moveg} = m_{move} + \frac{3}{2}m_c
\end{aligned}$$

2.4. Multi-Constraint Time Optimal Trajectory Planning

The trajectory of a plug seedling transplant is a continuous multipoint curve in the Cartesian coordinate system. The curve is discretized to several key points, and the sequence is $\{Q_i | i = 0, 1, 2, \cdots, 6\}$, where $Q_i = (x_i, y_i, z_i)$ is the coordinate point of the discrete point in the Cartesian coordinate system, as shown in Figure 7.

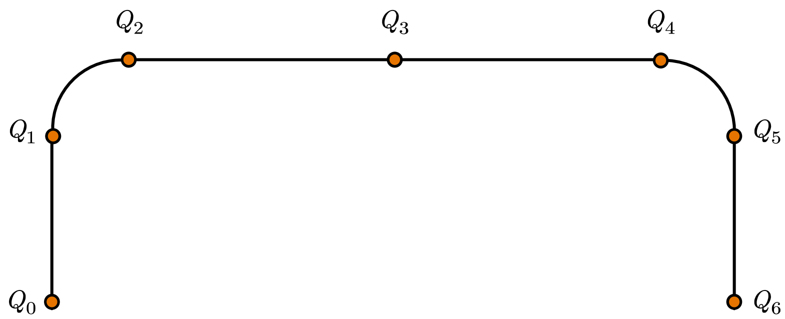

Figure 7. Trajectory discrete point sequence.

To avoid interference with other seedlings in the process of removing and supplementing seedlings, $Q_0 - Q_1$ and $Q_5 - Q_6$ are set as heights of 100 mm that need to be lifted and lowered, $Q_1 - Q_2$ and $Q_4 - Q_5$ are set as arc segments with a radius of 50 mm, Q_0 is the starting point, and Q_6 is the placement point.

The key nodes are obtained through the kinematic inverse solution to obtain the joint node sequence $P_i = [\theta_{1i}, \theta_{2i}, \theta_{3i}]$.

The 5th degree B-spline curve has the advantages of geometric invariance and local support, which can reduce the impact of the machine joint in the running process and at the same time can smoothly connect the multisection trajectory so that the adaptability of the whole trajectory is better. The joint space and time node is $\{P_i, t_i\}, i = 0, 1, \cdots, 6$, where t_i is the time node. B-spline interpolation curve planning is required for the B-spline curve to pass through target key nodes [29]. The kth degree B-spline curve function can be expressed as:

$$Q(u) = \sum_{i=0}^{n} d_i N_{i,k}(u), u \in [0, 1] \tag{9}$$

There are $n + 1$ control points $d_j (i = 0, 1, \cdots, n)$ and a node vector $U = \{u_0, u_1, \cdots u_{n+k+1}\}$ in the formula. The node vector u_i takes the value range of $[0, 1]$ in general, and $[u_0, u_1, \cdots, u_{n+k+1}]$ is a nondecreasing sequence. $N_{i,k}(u)$ is the kth degree B-spline basis function, which can be defined according to the Cox–de Boor recursive formula:

$$\begin{cases} N_{i,0}(u) = \begin{cases} 1 u_i \le u \le u_{i+1} \\ 0 \text{ other.} \end{cases} \\ N_{i,k}(u) = \frac{(u-u_i)N_{i,k-1}(u)}{u_{i+k}-u_i} + \frac{(u_{i+k+1}-u)N_{i+1,k-1}(u)}{u_{i+k+1}-u_{i+1}} \\ \text{stipulate} \frac{0}{0} = 0 \end{cases}$$

In the formula, the domain of $N_{i,k}$ is $(u_i, u_{i+k+1}]$, and the kth degree B-spline curve of nodes outside the interval is zero. The rth order derivative of the point on the B-spline curve is shown below:

$$Q^r(u) = \sum_{j=i-k}^{i-r} d_j^r N_{i,k}(u), u \in [u_i, u_{i+1}]$$
$$d_j^l = \begin{cases} d_j, l = 0 \\ (k-l+1)\frac{d_{j+1}^{l-1} - d_j^{l-1}}{u_{j+k+1} - u_{j+1}}, & \begin{matrix} l = 1,2,\cdots,r \\ j = i-k, i-k+1, \cdots, i-r \end{matrix} \end{cases} \tag{10}$$

Since the segmental connection point is equal to the key node, 7 equations are obtained by substituting the joint position, and then the derivatives of the start and end points are obtained through Equation (10), giving a total of 11 equations, as shown in Equation (11).

$$\begin{cases} Q(u_{i+5}) = Q_i \\ Q'(u_{i+5}) = Q'(u_{n+5}) = 0 \\ Q''(u_{i+5}) = Q''(U_{n+5}) = 0 \end{cases} \tag{11}$$

where $Q'(u)$ and $Q''(u)$ are the velocity and acceleration trajectory curves of the joints, respectively.

The solution is streamlined to Equation (12).

$$C_m d_m = Q_m \tag{12}$$

C_m is an 11×11 coefficient matrix; let $C_m(i,j)$ be the element of row i and column j. $C_m(i,j) = N_{i+j-3,5}(u_{i+4}), i = 2,3,\cdots,6$ and $j = i, i+1, \cdots, i+4$. The values of the other elements are related to the starting and ending node velocity and acceleration.

Thus, the trajectory control vertices of the 5th degree B-spline curve can be obtained, as shown in Equation (13).

$$d_m = C_M^{-1} Q_m \tag{13}$$

The function of the 5th degree B-spline curve with respect to time can be obtained by obtaining the control point and the node with respect to time. The overall performance of the curve can be optimized by dynamic adjustment of the time node sequence $\{t_1, t_2, t_3, t_4, t_5\}$.

To achieve the goal of the shortest operation time under the conditions of satisfying the constraints of kinematics, dynamics and terminal acceleration, the constructed objective function is shown in Equation (14).

$$\begin{cases} \left|\theta'(t)\right| \le V_{\max} \\ |\theta''(t)| \le A_{\max} \\ \tau \le \tau_{\max} \\ a_{move} \le a_{\max} \end{cases} \tag{14}$$

where $t \in [t_i, t_{i+1}]$ and $V_{\max}, A_{\max}, \tau_{\max}, a_{\max}$ represent the maximum velocity, acceleration, moment constraint, and maximum acceleration of the end of the active arm, respectively.$V_{\max} = 720°/\text{s}$, $A_{\max} = 2500°/\text{s}^2$, $\tau_{\max} = 12\ \text{N} \cdot \text{m}$, and $a_{\max} = 30\ \text{mm/s}^2$ according to the parameters obtained after motor selection.

The time least optimized objective function is established as shown in Equation (15).

$$\min(t) = \sum_{i=0}^{5} (t_{i+1} - t_i) \tag{15}$$

Particle swarm optimization (PSO) is an evolutionary computational algorithm with a simple structure. The parameters are easy to adjust with fast convergence, but PSO is prone to prematurity and a weak global optimum search [30]. In the N-dimensional search space, it is assumed that there are m particles in total, and each particle has a position and velocity. The current position of the ith particle can be expressed as $x_i = (x_{i1}, x_{i2}, \cdots, x_{id})$, $i = 1, 2, \cdots, m$, and the velocity can be expressed as $v_i = (v_{i1}, v_{i2} \cdots, v_{id})$. The fitness function calculates that each particle has the current optimal position expressed as p_{best}, and the optimal position of the entire particle swarm is expressed as g_{best}. The standard PSO algorithm is shown in Equation (16).

$$\begin{aligned} v_{id}^{t+1} &= \omega v_{id}^{t} + c_1 r_1 (p_{id}^{t} - x_{id}^{t}) + c_2 r_2 (p_{(i-1)d}^{t} - x_{id}^{t}) \\ x_{id}^{t+1} &= x_{id}^{t} + v_{id}^{t+1} \end{aligned} \tag{16}$$

where ω is the inertia weight. c_1 and c_2 are learning factors, also known as acceleration constants. r_1 and r_2 are random numbers between $[0, 1]$. v_{id}^{t} represents the dth component of the tth iteration speed of the ith particle, and x_{id}^{t} represents the dth component of the tth iteration position of the ith particle.

The artificial fish swarm algorithm (AFSA) has the advantage of being able to quickly jump out of the local extremum, but the convergence speed is slow in the latter operation [31]. The specific description of the four behaviors of artificial fish can be expressed as:

(1) Foraging behavior: the current state X_i of artificial fish will randomly select another state X_j within its sensing range, and the fitness functions Y_i and Y_j are calculated and compared under the two states. If $Y_j > Y_i$, X_i moves toward X_j. Otherwise, X_i continues to search within its sensing range to determine whether the movement requirements are met. The fitness functions Y_i of X_i and Y_j of X_j are calculated and compared. If the conditions are met, it moves toward X_j to X_{next}, which is represented by Equation (17).

$$X_{next} = X_i + rand() \times step \times \frac{X_j - X_i}{\|X_j - X_i\|} \tag{17}$$

where X_{next} is the next position of X_i. $step$ is the step length, and $rand()$ is a random number between $[0, 1)$.

If the condition is not met, search is conducted within the sensing range.

$$X_{next} = X_i + rand() \times step \tag{18}$$

(2) Clustering behavior: the artificial fish X_i will search for the number of peers N_f within its perception range and the center position X_c. If the condition $Y_c / N_f > \delta Y_i$ is met and δ is the congestion factor, it indicates that the position of its center peers is rich in food and not too crowded. It moves toward the partner's position once, as shown in Equation (19).

$$X_{next} = X_i + rand() \times step \times \frac{X_c - X_i}{\|X_c - X_i\|} \tag{19}$$

(3) Tail-chasing behavior: the artificial fish X_i searches for the number of companions N_f within its perceptual range and the optimal companion X_j, and if $Y_c / N_f > \delta Y_i$, it moves once toward the companion's position, which can be expressed as Equation (20).

$$X_{next} = X_i + rand() \times step \times \frac{X_j - X_i}{\|X_j - X_i\|} \tag{20}$$

(4) Random behavior: the purpose is to enable the population to expand the search range and facilitate jumping out of local optima. It can be expressed as Equation (21).

$$X_{next} = X_i + rand() \times visual \tag{21}$$

Integrating the two algorithms, we first use the global optimization ability of the AFSA to narrow the range of the solution domain and then use the advantage of PSO to quickly perform a local search in a small range to obtain a solution that is both fast and globally optimal.

(1) The spatial positions of the start and end points are obtained, the 5 transition points of the pick-fill trajectory are calculated, and these 7 points are imported into the kinematic inverse solution model to obtain the angle values in joint space.
(2) Parameters such as the number of artificial fish, sensing range, congestion, particle inertia weight, learning factor, and number of iterations are set.
(3) The 5th B-sample curve is used to connect the adjacent discrete points to determine whether the constraints are satisfied, and the artificial fish that meet the conditions are selected for the four behaviors. After each operation, comparison with the bulletin board is conducted, and the bulletin board is updated according to the best one, until the maximum number of iterations is reached, or it is within the allowable error range.
(4) The position in the end state of the artificial fish swarm is assigned to the particle swarm, the particle initialization speed in the particle swarm is given, and the adjacent discrete points connected with the 5th degree B-spline curve are used to judge whether the constraint conditions are met and whether compliant particles are used to calculate the fitness. The speed (p_{best}) and position (g_{best}) of the particle are updated according to Equation (16).
(5) The time-optimal sequence after the end condition is satisfied is the output. The starting point coordinate is randomly selected as $[-200, -200, -800]$, the ending point coordinate is randomly selected as $[250, 175, -800]$, and the units are mm. The population size of the artificial fish swarm is set to 20, the perception range is set to 2, the congestion is set to 0.6, the particle inertia weight is set to $w = 0.6$, the learning factors c_1 and c_2 are set to 5, and the number of iterations is set to 120. To verify the effectiveness of the hybrid algorithm, PSO, AFSA, and PSO–AFSA are compared in terms of the time-optimized solution of random points, as shown in Figure 8.

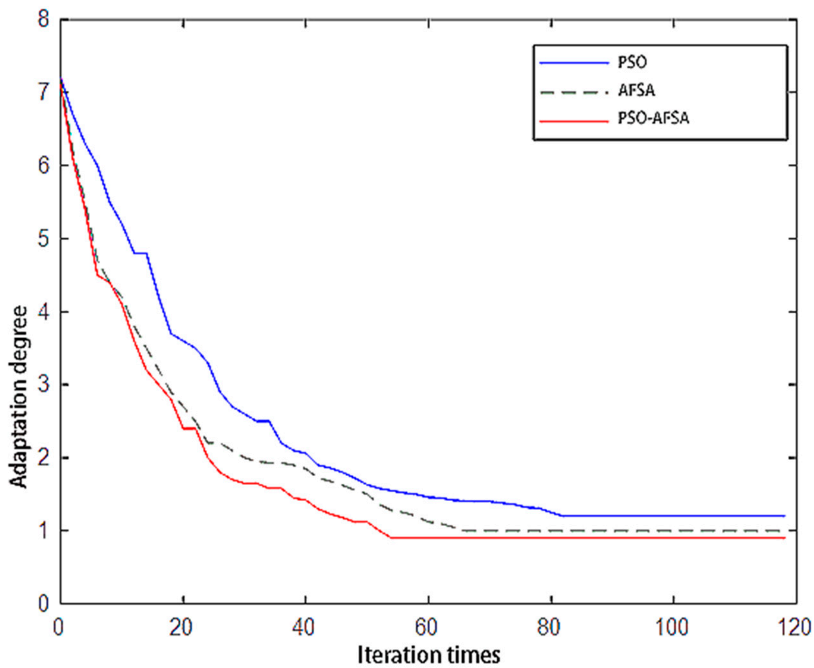

Figure 8. Comparison of the optimization iterations of the three algorithms.

After 57 iterations of PSO–AFSA, the optimal node sequence is $[0.21, 0.15, 0.18, 0.17, 0.15, 0.19]$, and the total time is 1.05 s. Compared with those of PSO and AFSA, the optimal time is increased by 30.48% and 12.38%, respectively. Compared with the other two algorithms, it is easier to eliminate the defect of falling into a local optimum.

The angle, angle velocity, angle acceleration, and end acceleration of each driving joint are obtained, as shown in Figures 9–13. During the test, each drive joint passed through 7 discrete points. At the same time, the velocity and acceleration of the start and end points are 0, and the velocity change is relatively slow when starting and stopping. During movement, the acceleration curve is continuous and smooth, which can effectively reduce the vibration effect on the overall mechanism. In terms of the degree of optimization, the actual running torque of the motor and the acceleration of the end are both close to the limit position ($\tau_{r\max} = 10.23\ \mathrm{N \cdot m}$ and $a_{r\max} = 29.87\ \mathrm{mm/s^2}$). It is shown that the optimization algorithm is more thorough for time optimization and avoids the problem encountered by ordinary optimization algorithms of falling into the local optimality after being far from the constraints and failing to reach the global optimum.

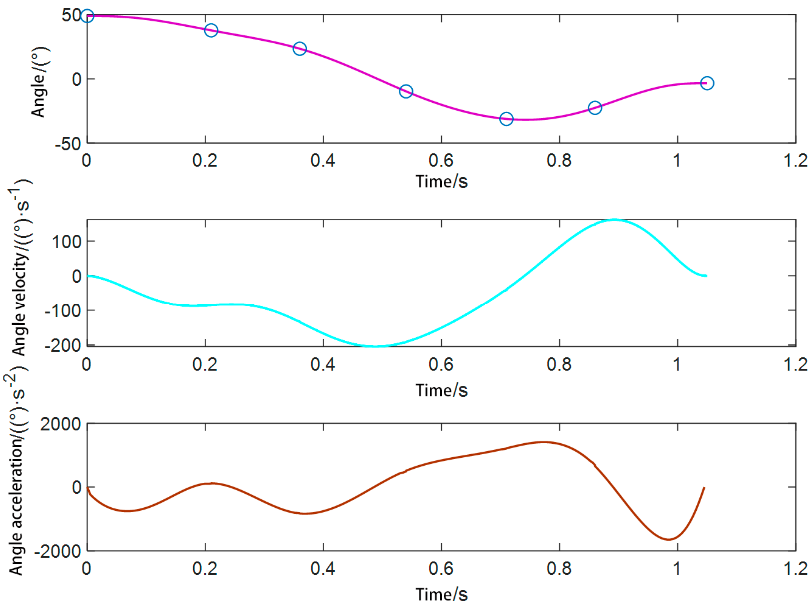

Figure 9. Plot of the angle, angle velocity, and angle acceleration of joint 1.

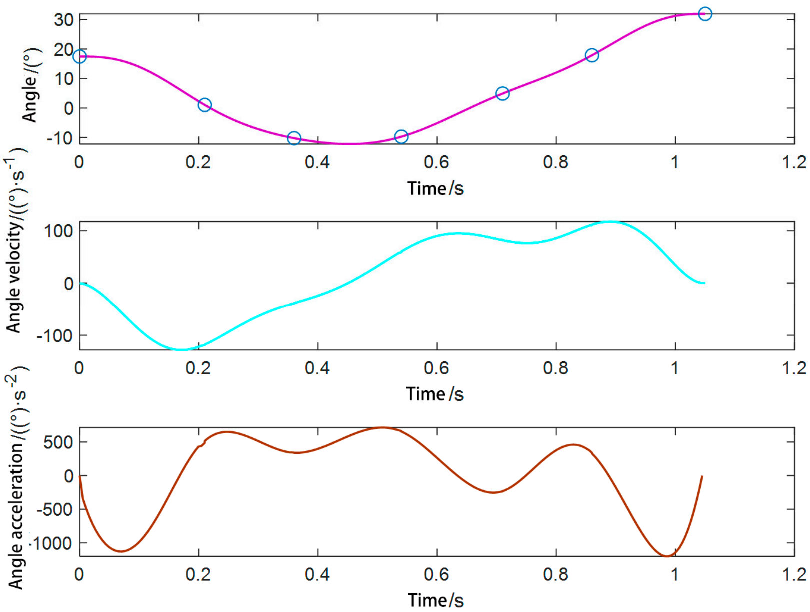

Figure 10. Plot of the angle, angle velocity, and angle acceleration of joint 2.

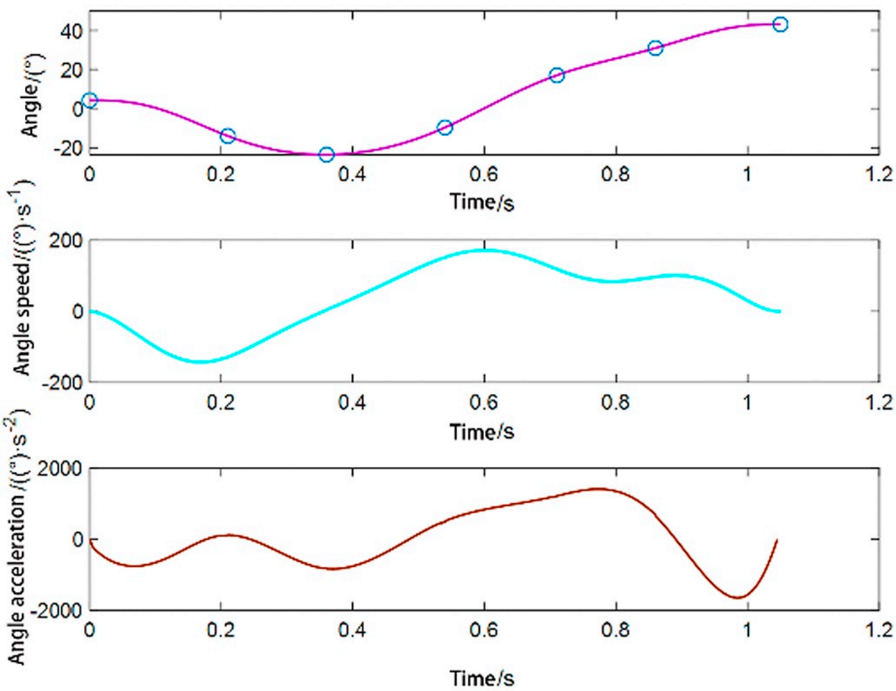

Figure 11. Plot of the angle, angle velocity, and angle acceleration of joint 3.

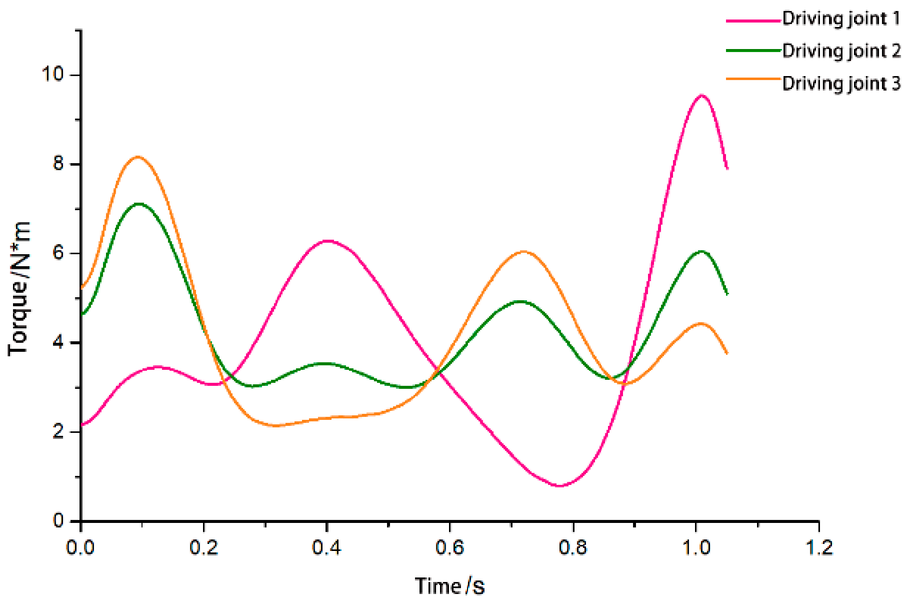

Figure 12. Torque change of each driving joint.

To verify the generality of the algorithm, tests were performed between 256 standard points in the working interval of the seedling supply and planting trays. The time of the robot operation in a single time does not exceed 1.36 s, regardless of the clamping and loosening time of the end effector. Since the position of each hole on the tray is fixed in the Cartesian coordinate system of the robot, when the delta robot operates, the planned operation scheme of the standard points in the corresponding area can be queried online, and the online optimization algorithm is not needed, which can greatly reduce the online operation time.

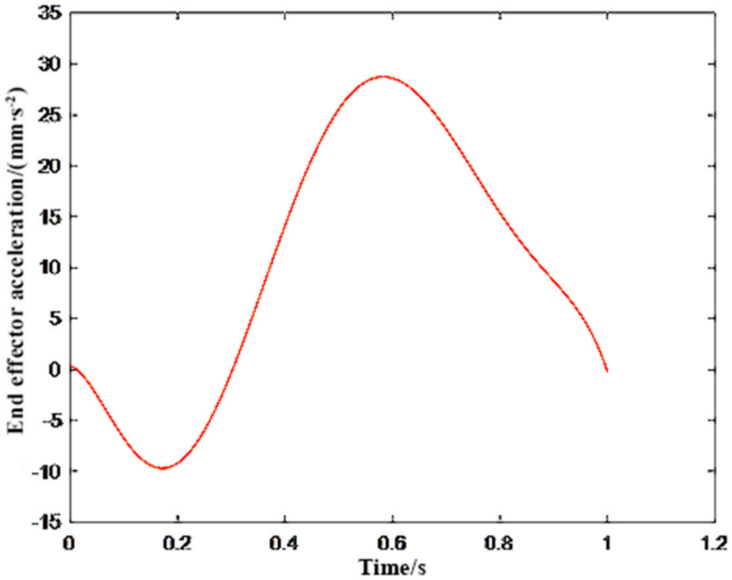

Figure 13. End effector acceleration variation.

3. Results and Discussion

Construction and Testing of the Machine

As is shown in Figure 14, the hardware system of the whole transplanting equipment is composed of a delta robot body, conveyor belt, and vision system, and the platform is built by the upper machine and lower machine. The processing of vision and trajectory planning are completed using MATLAB, and the control commands are sent to the PLC through communication. The PLC controller sends the corresponding pulse signals to the servo driver, which controls the operation of the servo motor and monitors the motor status. In this paper, a Siemens S7-1200 Smart PLC was selected. According to the target parameters of the robot, including the torque, inertia, power, etc., a pulse type Panasonic MSMF082L1U2M was selected as the servo motor.

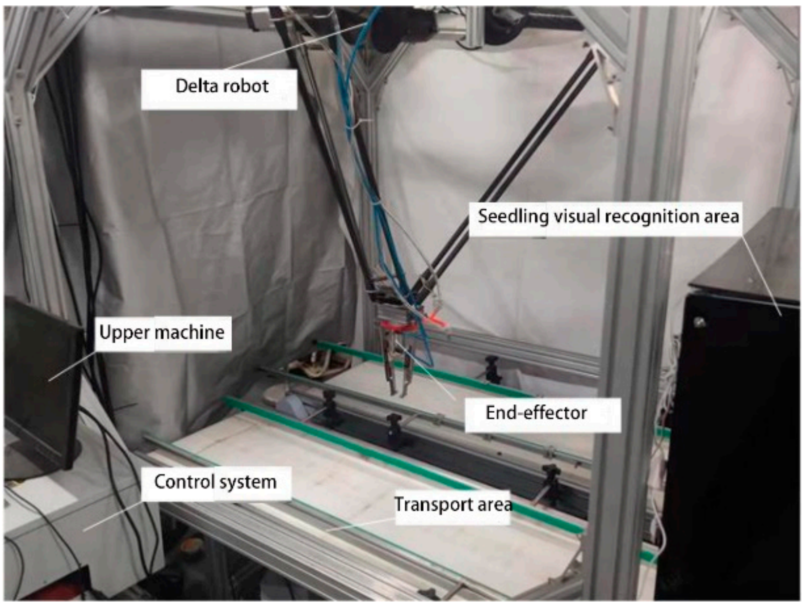

Figure 14. Whole machine physical diagram.

The specific process of the whole machine is as follows:

(1) The conveyor belt of the supplying tray and the planting tray is started. The two trays are placed on the corresponding conveyor belt intermittently, the photoelectric sensor detects that the tray is in place, and the two conveyor belts are stopped. The PLC sends the signal to the PC to carry out the image acquisition operation, the supplying tray and the planting tray are marked, the image is processed, the trajectory planning operation is carried out, and the data are saved for transmission to the PLC.
(2) After a delay of nearly 2 s, the tray conveyor is restarted. After reaching the photoelectric sensor, the conveyor stops running. First, seedling picking operations are carried out, inferior seedlings are recycled, and then seedlings are replenished. When the end effector starts to move along the trajectory discrete point sequence, the orientation start to work at the same time.
(3) The robot resets after finishing the operation on a tray of seedlings, processes the image of the next tray and overwrites the last data, and gives a signal to the conveyor belt when the supply tray is exhausted to start the supply conveyor belt until the next supply tray is supplied.

The above operations are cycled; the removal and supplementation operation is shown in Figure 15.

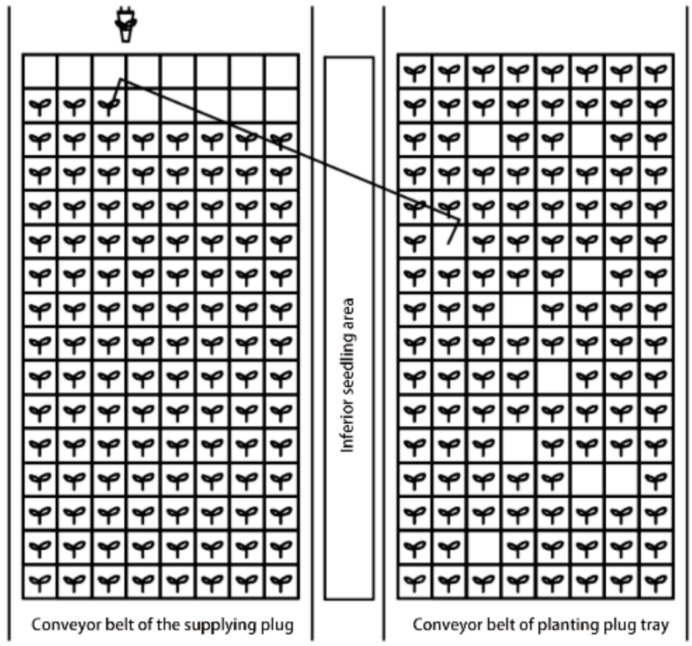

Figure 15. Schematic diagram of removing and supplementing plug seedlings in trays.

A test was prepared to cultivate one plate of inferior seedlings (without seed substrates) and eight plates of healthy seedlings. The seedlings were provided by the company Hangzhou Xiaomiao. The humidity of the seedlings we used was 60–70%, and the seedling age was 25 days. The seedling supply trays are all healthy seedlings, marked as A1, and the remaining five trays are marked as B1–B5. The transplanting performance test data are shown in Table 4.

Table 4. Data table of the transplanting test efficiency.

Tray No.	Time for a Single Removal and Supplementation Operation/s	Seedling Transplanting Efficiency/Plant/h	Tray Completion Productivity/Tray/h
B1	3.2	2459.6	75.6
B2	2.9	2698.4	79.8
B3	3.2	2426.8	75.4
B4	3.0	2563.4	78.7
B5	3.1	2503.2	76.6
Average value	3.1	2530.3	77.2

In another experiment, to verify the recognition effect of the growth information and pose judgement of the plug seedlings, the remaining two trays B6 and B7 were tested. The seedlings are transplanted from the two trays to the cavity tray, where B6 is the tray that has been judged by the pose and B7 is the tray that has not been judged by the posture. The number of intact leaves and the number of damaged leaves were counted to obtain the corresponding damage rate, as shown in Table 5.

Table 5. Comparison table of the injury before and after position posture judgement.

Tray No.	Number of Intact Leaves/Plant	Number of Damaged Leaves/Plant	Leaf Damage Rate/%
B6	120	8	6.25
B7	85	43	33.59

According to the test, the damage rate of the B7 pit plate is more than five times that of the B6 pit plate, which indicates that the position and posture judgement of seedling growth can effectively help to avoid seedling damage and ensure the integrity of leaves in the process of seedling trimming. The whole test process is shown in Figure 16, the transplanting diagram of healthy seedlings and inferior seedlings is shown in Figure 17, and the comparison of the effect before and after transplanting is shown in Figure 18.

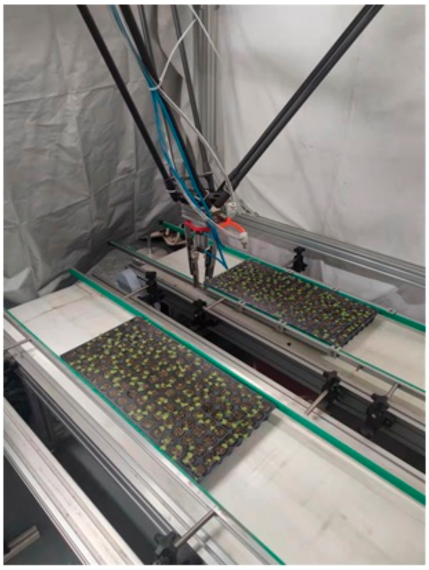

Figure 16. Transplanting process of the whole machine.

The overall test works well: the substrate of inferior seedlings can be completely removed, and there is no drop phenomenon during the transplanting process. After removing and supplementing the seedlings, the pot seedlings remained upright with less loss of substrates, and the leaves of the seedlings basically maintained the same state as before transplanting.

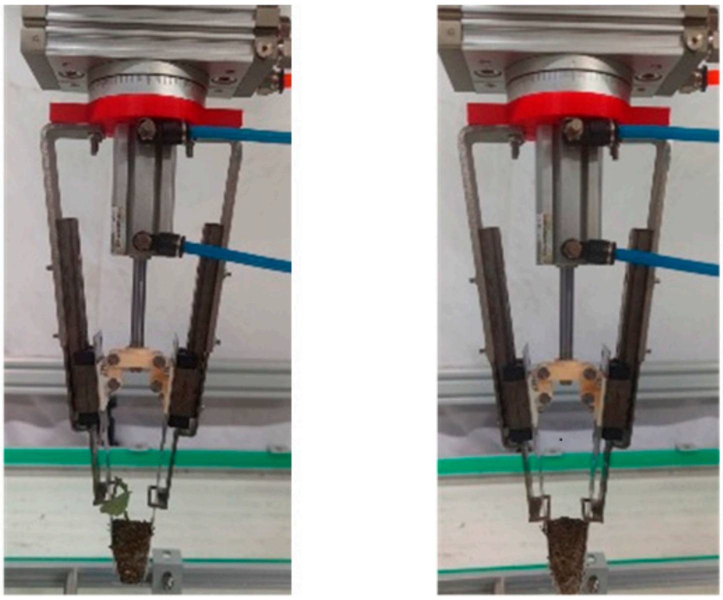

Figure 17. Transplantation of healthy and inferior seedlings.

Figure 18. Comparison of effects before and after transplanting: (**a**) tray condition before transplanting and (**b**) tray condition after transplanting.

4. Conclusions

(1) A closed image acquisition system was set up, and the obtained tray images were tilt-corrected and the internal wireframe was extracted to extract the seedling leaf features and make out-of-bound judgements based on the positional relationship between the leaves and tray wireframes. The plug seedlings were divided into four categories according to the leaf area and the direction of seedling crossing.

(2) A kind of cylinder-driven plug-in end effector was designed, which was connected to a reciprocating 90° rotary cylinder to meet the needs of transplanting seedlings with different growth positions and postures. Taking broccoli seedlings at the cotyledon stage as the transplanting object, a three-level and three-factor orthogonal test was conducted. The optimal combination of parameters was as follows: substrate moisture content of 60–70%, seedling age of 25 days, and transplanting acceleration of 30 mm/s^2.

(3) Using the PSO–AFSA algorithm to search for the optimal time, the single operation time of the robot did not exceed 1.36 s without considering the end-effector clamping and releasing action time in the test.

(4) The whole machine was systematically built, the average time of a single seedling removal and supplementation procedure was 3.1 s, and the transplanting efficiency of the whole machine was 2530.3 plants/h. The seedling damage rates with and without pose recognition were tested, and the leaf damage rates were 6.25% and 33.59%, respectively.

Author Contributions: Conceptualization, X.Z. and W.D.; methodology, W.D. and D.C.; software, X.M.; validation, D.C., W.D. and X.M.; formal analysis, D.C.; investigation, X.M.; resources, D.C.; data curation, X.M.; writing—original draft preparation, W.D.; writing—review and editing, X.M.; visualization, X.Z.; supervision, X.Z.; project administration, Y.X.; funding acquisition, J.T. All authors have read and agreed to the published version of the manuscript.

Funding: This research was funded by the National Natural Science Foundation of China (grant number 32071909, 51975536), the Key Research Projects of Zhejiang Province (grant number 2022C02002), the Basic Public Welfare Research Projects of Zhejiang Province (grant number LGN20E050006), the Shanghai Science and technology agricultural Development Project 2021 (number 4–1), and the General Project of Agriculture and Social Development in Hangzhou (grant number 20201203B92).

Institutional Review Board Statement: Not applicable.

Informed Consent Statement: Not applicable.

Data Availability Statement: The data presented in this study are available upon request from the corresponding author.

Conflicts of Interest: The authors declare no conflict of interest.

References

1. Xin, Z.; Cui, Y.; Yang, X.; Kong, L.; Lin, Q. Current Situation of Global Vegetable Industry and Research Progress of Vegetable Breeding Development Path in China. *Mol. Plant Breed.* **2022**, *20*, 3122–3132.
2. Jin, X.; Tang, L.; Li, R.; Zhao, B.; Ji, J.; Ma, Y. Edge recognition and reduced transplantation loss of leafy vegetable seedlings with Intel RealsSense D415 depth camera. *Comput. Electron. Agric.* **2022**, *198*, 107030. [CrossRef]
3. Choi, W.C.; Kim, D.C.; Ryu, I.H.; Kim, K.U. Development of a seedling pick-up device for vegetable transplanters. *Trans. Am. Soc. Agric. Eng.* **2002**, *45*, 13–19.
4. Wen, Y.; Zhang, J.; Tian, J. Design of a traction double-row fully automatic transplanter for vegetable plug seedlings. *Comput. Electron. Agric.* **2021**, *182*, 106017. [CrossRef]
5. Paradkar, V.; Raheman, H.; Rahul, K. Development of a metering mechanism with serial robotic arm for handling paper pot seedlings in a vegetable transplanter. *Artif. Intell. Agric.* **2021**, *5*, 52–63. [CrossRef]
6. Li, H.; Li, Z.; Dong, W.; Cao, X.; Wen, Z.; Xiao, R.; Wei, Y. An automatic approach for detecting seedlings per hill of machine-transplanted hybrid rice utilizing machine vision. *Comput. Electron. Agric.* **2021**, *185*, 106178. [CrossRef]
7. Yang, Y.; Huang, G.; Shi, X.; He, M.; Ahmad, I.; Zhao, X. Design of a control system for a mini-automatic transplanting machine of plug seedling. *Comput. Electron. Agric.* **2020**, *169*, 105226. [CrossRef]
8. Bai, J.; Hao, F.; Cheng, G. Machine vision-based supplemental seeding device for plug seedling of sweet corn. *Comput. Electron. Agric.* **2021**, *188*, 106345. [CrossRef]
9. Wang, Y.; Xiao, X.; Liang, X. Plug hole positioning and seedling shortage detecting system on automatic seedling supplementing test-bed for vegetable plug seedlings. *Trans. Chin. Soc. Agric. Eng.* **2018**, *34*, 35–41.
10. Shao, Y.; Han, X.; Xuan, G.; Liu, Y.; Gao, C.; Wang, G. Development of a multi-adaptive feeding device for automated plug seedling transplanter. *Int. J. Agric. Biol. Eng.* **2021**, *14*, 91–96. [CrossRef]
11. Zhou, M.; Shan, Y.; Xue, X.; Yin, D. Theoretical analysis and development of a mechanism with punching device for transplanting potted vegetable seedlings. *Int. J. Agric. Biol. Eng.* **2020**, *13*, 85–92. [CrossRef]
12. Xue, X.; Li, L.; Xu, C.; Li, E.; Wang, Y. Optimized design and experiment of a fully automated potted cotton seedling transplanting mechanism. *Int. J. Agric. Biol. Eng.* **2020**, *13*, 111–117. [CrossRef]
13. Mao, H.; Han, L.; Hu, J.; Kumi, F. Development of a pincette-type pick-up device for automatic transplanting of greenhouse seedlings. *Appl. Eng. Agric.* **2014**, *30*, 547–556.
14. Yang, X.; Ma, Y. Current situation and development trend of vegetable mechanized seedling transplanting in facilities. *J. Agric. Mech. Res.* **2022**, *44*, 8–13+, 32.
15. Vafapour, R.; Gharib, M.R.; Honari-Torshizi, M.; Ghorbani, M. On the applicative workspace and the mechanism of an agriculture 3-dof 4-cable-driven robot. *Int. J. Robot. Autom.* **2021**, *1*, 36.
16. Tong, J.; Qiu, Z.; Zhou, H.; Bashir, M.K.; Yu, G.; Wu, C.; Du, X. Optimizing the path of seedling transplanting with multi-end effectors by using an improved greedy annealing algorithm. *Comput. Electron. Agric.* **2022**, *201*, 107276. [CrossRef]
17. Tong, J.; Ding, Y.; Wu, C.; Yu, Q.; Pan, J.H.; Sun, L. Design and experiment of key mechanism for semi-automatic vegetable grafting machine. *Trans. Chin. Soc. Agric. Mach.* **2018**, *49*, 65–72.
18. Tong, J.; Jiang, H.; Wu, C. Optimization of seedlings lower density transplanting path based on greedy algorithm. *Trans. Chin. Soc. Agric. Mach.* **2016**, *47*, 8–13.
19. Wen, Y.; Zhang, L.; Huang, X. Design of and Experiment with Seedling Selection System for Automatic Transplanter for Vegetable Plug Seedlings. *Agronomy* **2021**, *11*, 2031. [CrossRef]

20. Xin, J.; Kaixuan, Z.; Jiangtao, J.; Xinwu, D.; Hao, M.; Zhaomei, Q. Design and implementation of intelligent transplanting system based on photoelectric sensor and PLC. *Future Gener. Comput. Syst.* **2018**, *88*, 127–139. [CrossRef]
21. Hu, J.; Yan, X.; Ma, J.; Qi, C.; Francis, K.; Mao, H. Dimensional synthesis and kinematics simulation of a high-speed plug seedling transplanting robot. *Comput. Electron. Agric.* **2014**, *107*, 64–72. [CrossRef]
22. Shuangyan, H.; Minjuan, H.; Wenyi, Z. Design and experiment of flexible clamping device for pepper plug seedlings. *Adv. Mech. Eng.* **2022**, *14*, 168–176. [CrossRef]
23. Ndawula, I.; Assal, S. Conceptual design and kinematic analysis of a novel open field 3dof multi-gripper pot seedlings transplanting robot. In Proceedings of the 2018 IEEE International Conference on Mechatronics and Automation (ICMA), Changchun, China, 5–8 August 2018; IEEE: Piscataway, NJ, USA, 2018; pp. 1458–1463.
24. Zhang, S.; Tian, S.; Qiu, L. Structure design and simulation on manipulator of transplanting potted tray seedlings. *J. Shenyang Agric. Univ.* **2007**, *15*, 437–439. [CrossRef]
25. Jiang, Z.; Hu, Y.; Jiang, H. Design and force analysis of end-effector for plug seedling transplanter. *PLoS ONE* **2017**, *12*, 180–182. [CrossRef]
26. Zhang, S.; Yao, M.; Fan, L. Optimization of frying technology of Chrysanthemum by orthogonal test with multi-index comprehensive scoring method. *J. Tianjin Univ. Tradit. Chin. Med.* **2020**, *39*, 570–575.
27. Liu, G.; Chen, Y.; Xie, Z. GA\SQP optimization for the dimensional synthesis of a delta mechanism based haptic device design. *Robot. Comput.-Integr. Manuf.* **2018**, *51*, 73–84. [CrossRef]
28. Carbonari, L. Simplified approach for dynamics estimation of a minor mobility parallel robot. *Mechatronics* **2015**, *30*, 76–84. [CrossRef]
29. Li, Y.; Huang, T.; Chetwynd, D.G. An approach for smooth trajectory planning of high-speed pick-and-place parallel robots using quintic B-splines. *Mech. Mach. Theory* **2018**, *126*, 479–490. [CrossRef]
30. Li, X.; Serra, R.; Olivier, J. A multi-component PSO algorithm with leader learning mechanism for structural damage detection. *Appl. Soft Comput.* **2022**, *116*, 108315. [CrossRef]
31. Li, F.; Du, Y.; Jia, K.J. Path planning and smoothing of mobile robot based on improved artificial fish swarm algorithm. *Sci. Rep.* **2022**, *12*, 659. [CrossRef] [PubMed]